

Article

Active and Reactive Power Compensation Control Strategy for VSC-HVDC Systems under Unbalanced Grid Conditions

Weiming Liu ¹, Tingting Zheng ¹, Ziwen Liu ^{2,*}, Zhihua Fan ², Yilong Kang ², Da Wang ¹, Mingming Zhang ¹ and Shihong Miao ^{2,*}

¹ State Grid East Inner Mongolia Electric Power Research Institute, Hohhot 010020, China; liuweiming@md.sgcc.com.cn (W.L.); zhengtingting@md.sgcc.com.cn (T.Z.); wangda@md.sgcc.com.cn (D.W.); zhangmingming@md.sgcc.com.cn (M.Z.)

² State Key Laboratory of Advanced Electromagnetic Engineering and Technology, School of Electrical and Electronic Engineering, Huazhong University of Science and Technology, Wuhan 430074, China; fzhust@hust.edu.cn (Z.F.); ylkang@hust.edu.cn (Y.K.)

* Correspondence: liuziwen@hust.edu.cn (Z.L.); shmiao@hust.edu.cn (S.M.); Tel.: +86-027-87543228 (Z.L. & S.M.)

Received: 23 October 2018; Accepted: 8 November 2018; Published: 13 November 2018



Abstract: This paper presents a power compensation strategy to suppress the double frequency power ripples of Voltage source converter high-voltage direct current (VSC-HVDC) systems under unbalanced grid voltage conditions. The mathematical control equations of the double frequency ripple power of VSC under unbalanced operating conditions are firstly derived and established, where the dynamic behaviors of the double frequency ripples in active and reactive power are regarded as being driven by current-relevant components and voltage-relevant components, respectively. Based on the equations, a power compensation control strategy of VSC-HVDC is proposed via the passivity-based control with disturbance observer to suppress both the current-relevant and voltage-relevant components in the power ripples. With this control strategy, the double frequency ripples in active and reactive power are suppressed simultaneously and system performance is significantly enhanced with the implementation of the disturbance observer in the passivity-based control. Theoretical stability analysis and simulation cases show the effectiveness and superiority of the proposed strategy.

Keywords: VSC-HVDC; unbalanced grid conditions; double frequency ripples; power compensation; passive-based control; disturbance observer

1. Introduction

Recently, the voltage source converter based high voltage direct current (VSC-HVDC) is widely used in dc transmission, renewable energy generation, island network supply and other fields [1–4]. In general control scheme of VSC-HVDC, the three-phase AC grid voltage is usually assumed to be balanced. However, once the unbalanced grid conditions occur (e.g., due to AC grid voltage unbalance and unsymmetrical faults), the converter will operate in abnormal condition and the negative sequence components in voltage and current will do great harm to system operation. If no compensation measures are adopted, the double frequency ripples will appear in the output power of VSC, which affects output quality of the converter [5–7] and may even make the converter malfunction. Therefore, how to suppress the double frequency ripples under unbalanced grid conditions becomes a hot topic in the research of VSC-HVDC control.

To suppress the double frequency power ripples, the additional active power filter is utilized in Reference [8–10] to eliminate the asymmetric components. The active power filter has ideal performance in regulating asymmetrical components but the cost input is high. Hence improving the control strategy of the converter is the mainstream research on the suppression of double frequency power ripples. The VSC control strategies in ideal balance grid have been relatively mature and the most common schemes are the voltage oriented control (VOC). The existing unbalance control research of VSC under the framework of VOC is mainly realized by obtaining the control reference value according to some kind of control objective (e.g., elimination of active power ripple, reactive power ripple or negative-sequence current component) and tracking this reference value with suitable method [11,12]. In Reference [13], a novel method of separating the instantaneous positive and negative sequence components is proposed and well applied for different control objectives of VSC under unbalanced grid voltage. In Reference [14], an optimal active and reactive power control is proposed to achieve multi-objectives for VSC-HVDC under unbalanced grid voltage conditions. A flexible control strategy is proposed in Reference [15] for oscillation control of the active and reactive power by introducing a control parameter k . In Reference [16], an improved model predictive current control for VSC is presented when unbalanced grid voltages occur to reduce power fluctuations. In Reference [17], a direct power control for grid-connected VSC under unbalanced network is proposed by applying a virtual phase angle for coordinated transformations. The optimal power control strategies for VSC-HVDC systems under unbalanced grid voltage conditions are proposed in Reference [18,19], which enable the system to provide flexible power control. In Reference [20], a power control of VSC-HVDC converters is presented to limit the influence of AC unbalanced faults on multi-terminal DC grids. In Reference [21], a novel unified dynamic model and control strategy are presented to improve the power quality for VSC-HVDC under unbalanced grid conditions. These control strategies are verified to be effective but the fluctuations of active and reactive power cannot be suppressed at the same time.

For past few years, the passivity-based control has attracted more and more attentions because of the flexible adjustment and simplified control structure and has been applied in power converter control [22,23]. The passivity-based control of the doubly fed induction generator under unbalanced grid voltage is proposed in Reference [24]. However, the passivity-based control is applied to replace the traditional PI (Proportional-Integral) control for system response improvement instead of eliminating the double frequency ripple power. Therefore, the double frequency ripples in active and reactive power still cannot be suppressed simultaneously. On the other hand, although the passivity-based control gives the controller design by configuring system energy and injecting damping to achieve the satisfactory transient response, it is sensitive to unmodeled dynamics and model errors. To handle the issue, a perturbation observer-based passivity-based control is proposed in Reference [25] but the implementation of high-order observer brings in serious noise and complicates system structure, which means the enhanced passivity-based control also needs further study.

In this paper, a power compensation strategy to suppress the double frequency ripples in active and reactive power of VSC-HVDC systems under unbalanced grid voltage conditions is proposed. The main work of this paper can be drawn as:

- (1) The mathematical control equations of the double frequency ripple power of VSC under unbalanced grid conditions are derived and established. In the equations, the dynamic behaviors of the double frequency ripples in active and reactive power are regarded as being driven by current-relevant components and voltage-relevant components, which can be controlled respectively for double frequency ripple suppression.

- (2) Based on the established control equations, a power compensation control strategy of VSC-HVDC is proposed via the passivity-based control with disturbance observer. The passivity-based control is responsible for the tracking control of current-relevant components with the expected value, while the disturbance observer focuses on the compensation of the voltage-relevant components. With this control strategy, the double frequency ripples in active and reactive power of VSC-HVDC under unbalanced grid conditions are suppressed simultaneously and system

performance is significantly enhanced with the implementation of the disturbance observer in the passivity-based control.

Theoretical stability analysis and simulations of a two-terminal VSC-HVDC system on PSCAD/EMTDC verify the validity and superiority of the proposed control strategy.

2. Analysis and Control Equations Establishment of Double Frequency Ripple power of VSC

The VSC structure adopted in this paper is the two-level topology and shown in Figure 1. The representations of the variables in Figure 1 are shown in the Nomenclature Section. Although the modular multilevel converter (MMC) is recognized as the promising converter technology applied in high-voltage and high-power transmission technology, the system-level control of MMC is similar to that in two-level converter since they have same vector control model in dq coordinate system [26], which mean the response characteristics of the two converters under unbalanced grid conditions are also same. Therefore, the two-level converter is used as the study object in this paper for explicit explanations.

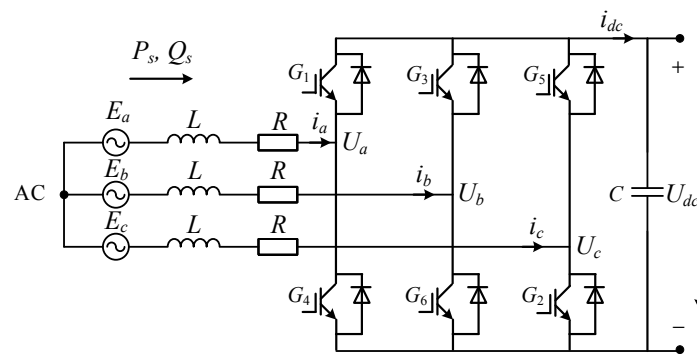


Figure 1. The VSC topological structure.

Under balanced grid voltage condition, the mathematical model of VSC in synchronous rotating reference frame is [11]

$$\begin{bmatrix} U_d \\ U_q \end{bmatrix} = \begin{bmatrix} E_d \\ E_q \end{bmatrix} - R \begin{bmatrix} i_d \\ i_q \end{bmatrix} - L \frac{d}{dt} \begin{bmatrix} i_d \\ i_q \end{bmatrix} + \omega L \begin{bmatrix} i_q \\ -i_d \end{bmatrix}, \quad (1)$$

When asymmetric fault occurs in the grid, the dissymmetry in system electrical quantities is mainly caused by negative sequence components, since the zero sequence components are isolated by the Y/Δ transformer in the grid side. Considering that in the synchronous rotating reference frame, the positive sequence component is equal to the dc component, while the negative sequence component is equal to the double frequency component, the double frequency ripple power in the forward direction dq rotating frame can be written as (2) according to [17] (*d* axis is chosen to be coincided with grid voltage vector)

$$\begin{cases} P_2 = \frac{3}{2}(i_{d0}E_{d2} + i_{q0}E_{q2} + E_{d0}i_{d2}) \\ Q_2 = \frac{3}{2}(i_{d0}E_{q2} - i_{q0}E_{d2} - E_{d0}i_{q2}) \end{cases}, \quad (2)$$

where the right subscript “0” stands for dc component and “2” stands for double frequency component. It is seen from (2) that the factors that cause the double frequency ripples in the output power include the double frequency components of grid voltage (E_{d2} and E_{q2}) and the double frequency components of VSC current (i_{d2} and i_{q2}). Therefore, the double frequency ripple power can be regard as the results driven by the current-relevant components and voltage-relevant components which can be described as

$$\begin{cases} P_2 = P_{2i} + P_{2u} \\ Q_2 = Q_{2i} + Q_{2u} \end{cases}, \quad (3)$$

where P_{2i} , P_{2u} , Q_{2i} and Q_{2u} are defined as

$$\begin{cases} P_{2i} = \frac{3}{2}E_{d0}i_{d2}, P_{2u} = \frac{3}{2}(i_{d0}E_{d2} + i_{q0}E_{q2}) \\ Q_{2i} = -\frac{3}{2}E_{d0}i_{q2}, Q_{2u} = \frac{3}{2}(i_{d0}E_{q2} - i_{q0}E_{d2}) \end{cases}, \quad (4)$$

To control double frequency ripple power, take the derivative of (4). Since the derivative of dc component is zero, it results in

$$\begin{cases} \frac{dP_2}{dt} = \frac{dP_{2i}}{dt} + \frac{dP_{2u}}{dt} = \frac{3}{2}E_{d0} \frac{di_{d2}}{dt} + \frac{dP_{2u}}{dt} \\ \frac{dQ_2}{dt} = \frac{dQ_{2i}}{dt} + \frac{dQ_{2u}}{dt} = -\frac{3}{2}E_{d0} \frac{di_{q2}}{dt} + \frac{dQ_{2u}}{dt} \end{cases}, \quad (5)$$

Since the independent control equation of VSC double frequency voltage can be derived as

$$\begin{bmatrix} U_{d2} \\ U_{q2} \end{bmatrix} = \begin{bmatrix} E_{d2} \\ E_{q2} \end{bmatrix} - R \begin{bmatrix} i_{d2} \\ i_{q2} \end{bmatrix} - L \frac{d}{dt} \begin{bmatrix} i_{d2} \\ i_{q2} \end{bmatrix} + \omega L \begin{bmatrix} i_{q2} \\ -i_{d2} \end{bmatrix}, \quad (6)$$

By substituting (6) into (5), it results in

$$\begin{cases} L \frac{dP_2}{dt} = \frac{3}{2}E_{d0}(E_{d2} - Ri_{d2} - U_{d2} + \omega Li_{q2}) + L \frac{dP_{2u}}{dt} \\ L \frac{dQ_2}{dt} = -\frac{3}{2}E_{d0}(E_{q2} - Ri_{q2} - U_{q2} - \omega Li_{d2}) + L \frac{dQ_{2u}}{dt} \end{cases}, \quad (7)$$

Furtherly, the differential equations which take double frequency power P_2 and Q_2 as state variables can be obtained as

$$\begin{cases} L \frac{dP_2}{dt} = \frac{3}{2}E_{d0}E_{d2} - RP_2 - u_P - \omega LQ_2 + \left(L \frac{dP_{2u}}{dt} + RP_{2u} + \omega LQ_{2u} \right) \\ L \frac{dQ_2}{dt} = -\frac{3}{2}E_{d0}E_{q2} - RQ_2 + u_Q + \omega LP_2 + \left(L \frac{dQ_{2u}}{dt} + RQ_{2u} - \omega LP_{2u} \right) \end{cases}, \quad (8)$$

where u_P and u_Q satisfy $u_P = 1.5E_{d0}U_{d2}$, $u_Q = 1.5E_{d0}U_{q2}$. Let w_{Pu} and w_{Qu} be defined as

$$\begin{cases} w_{Pu} = \frac{3}{2}E_{d0}E_{d2} + L \frac{dP_{2u}}{dt} + RP_{2u} + \omega LQ_{2u} \\ w_{Qu} = -\frac{3}{2}E_{d0}E_{q2} + L \frac{dQ_{2u}}{dt} + RQ_{2u} - \omega LP_{2u} \end{cases}, \quad (9)$$

In (9), the voltage-relevant components that cause the double frequency power ripples are included in w_{Pu} and w_{Qu} , which can be regarded as the “double frequency voltage disturbance” of the differential Equations (8). Meanwhile, to furtherly improve the robustness of control system, the error terms ε_P and ε_Q are introduced in the disturbances w_{Pu} and w_{Qu} to describe the unmodeled dynamics including modelling errors and unknown time-varying external disturbances. Then it yields that

$$\begin{cases} w_{Pu} = \frac{3}{2}E_{d0}E_{d2} + L \frac{dP_{2u}}{dt} + RP_{2u} + \omega LQ_{2u} + \varepsilon_P \\ w_{Qu} = -\frac{3}{2}E_{d0}E_{q2} + L \frac{dQ_{2u}}{dt} + RQ_{2u} - \omega LP_{2u} + \varepsilon_Q \end{cases}, \quad (10)$$

Finally, the control equations of the double frequency ripple power can be depicted by

$$\begin{cases} L \frac{dP_2}{dt} = -RP_2 - u_P - \omega LQ_2 + w_{Pu} \\ L \frac{dQ_2}{dt} = -RQ_2 + u_Q + \omega LP_2 + w_{Qu} \end{cases}, \quad (11)$$

In (11), w_{Pu} and w_{Qu} reflect the influence of voltage-relevant components and unmodeled dynamics on the double frequency ripple power. Apart from w_{Pu} and w_{Qu} , the control Equation (11) reflect the double frequency ripple behaviors caused by current-relevant components. Hence through proper double frequency power compensation control based on (11), the current-relevant and voltage-relevant components that cause double frequency ripples can be suppressed simultaneously.

3. Power Compensation Strategy for VSC-HVDC via Passivity-Based Control with Disturbance Observer

In normal condition, the common vector double loop control is adopted in VSC for desired control aims. However, under unbalanced grid voltage, a power compensation controller is needed to suppress the double frequency power ripples with no impact on the normal operation of VSC. The compensation strategy should be effective in controlling the double frequency components of the unbalanced voltage and current to compensate the output voltage of inner loop PI control. In this paper, the passivity-based control with disturbance observer are proposed to form the power compensation control, which serves as the auxiliary adjustment of VSC under unbalanced grid condition. The design of passivity-based control aims at minimizing the double frequency ripple power P_2 and Q_2 with the double frequency voltage disturbance w_{Pu} and w_{Qu} observed and compensated in the control scheme.

3.1. PCHD Model of the VSC-HVDC Systems and the Passivity-Based Control Strategy

Consider the PCHD (Port-Controlled Hamiltonian with Dissipation) model [23] of control Equation (11) described as

$$\begin{cases} \dot{x} = [J(x) - \mathfrak{R}(x)] \frac{\partial H(x)}{\partial x} + G(x)u \\ y = G^T(x) \frac{\partial H(x)}{\partial x} \end{cases}, \quad (12)$$

where $x(t)$, $u(t)$ and $y(t)$ denote the system state, the control input and the system output, respectively. It is noted that with the positive defined Hamiltonian function $H(x)$ to be system storage function, the system (12) is passive from the input u to output y . The system state and input variables are shown as

$$\begin{cases} x = [LP_2 \quad LQ_2]^T = D[P_2 \quad Q_2]^T, \quad u = [u_1 \quad u_2]^T \\ D = \begin{bmatrix} L & 0 \\ 0 & L \end{bmatrix}, \quad G = \begin{bmatrix} -1 & 0 \\ 0 & 1 \end{bmatrix} \end{cases}, \quad (13)$$

The disturbance w_{Pu} and w_{Qu} is involved in the control input, which means $u_1 = u_P - w_{Pu}$ and $u_2 = u_Q + w_{Qu}$. Then the Hamiltonian function $H(x)$ are obtained as

$$H = \frac{1}{2} x^T D^{-1} x = \frac{1}{2} \left(\frac{1}{L} x_1^2 + \frac{1}{L} x_2^2 \right), \quad (14)$$

The interconnection matrix and damping matrix shown in (15) satisfy $J = -J^T$ and $\mathfrak{R} = \mathfrak{R}^T \geq 0$

$$J = \begin{bmatrix} 0 & -\omega L \\ \omega L & 0 \end{bmatrix}, \quad \mathfrak{R} = \begin{bmatrix} R & 0 \\ 0 & R \end{bmatrix}, \quad (15)$$

The control objective of the passivity-based control based on PCHD model is to seek a control input u to ensure that the closed-loop system (12) is asymptotically stable within the desired equilibrium point x^*

$$x^* = \begin{bmatrix} x_1^* & x_2^* \end{bmatrix}^T = \begin{bmatrix} LP_2^* & LQ_2^* \end{bmatrix}^T. \quad (16)$$

To achieve the control objective that system (12) can be asymptotically stable, a closed-loop desired Hamiltonian function $H_d(x)$ with the feedback control $u = \beta(x)$ should be considered so that system energy is minimum in the equilibrium point and that the system can be described by the equations.

$$\dot{x} = [J_d(x) - \mathfrak{R}_d(x)] \frac{\partial H_d(x)}{\partial x}, \quad (17)$$

where J_d and \mathfrak{R}_d satisfy

$$\begin{cases} J_d(x) = J(x) + J_a(x) = -J_d^T(x) \\ \mathfrak{R}_d(x) = \mathfrak{R}(x) + \mathfrak{R}_a(x) = \mathfrak{R}_d^T(x) \\ H_d(x) = H(x) + H_a(x) \end{cases}, \quad (18)$$

Designers should have high freedom in selecting the matrix J_d , \mathfrak{R}_d and H_d to satisfy the desired objective. For general speaking, it is defined that

$$\begin{cases} J_a = \mathbf{0} \\ \mathfrak{R}_a = \begin{bmatrix} r_1 & 0 \\ 0 & r_2 \end{bmatrix} \end{cases}, \quad (19)$$

The closed-loop desired Hamiltonian function $H_d(x)$ is taken as

$$H_d(x) = \frac{1}{2}(x - x^*)^T D^{-1}(x - x^*), \quad (20)$$

Then it can be obtained in (21) by substituting (18), (19) and (20) into (12)

$$\begin{aligned} \dot{x} &= [(J_d - J_a) - (\mathfrak{R}_d - \mathfrak{R}_a)] \left(\frac{\partial H_d(x)}{\partial x} - \frac{\partial H_a(x)}{\partial x} \right) + Gu \\ &= (J_d - \mathfrak{R}_d) \frac{\partial H_d(x)}{\partial x} - (J_a - \mathfrak{R}_a) \frac{\partial H(x)}{\partial x} - (J_d - \mathfrak{R}_d) \frac{\partial H_a(x)}{\partial x} + Gu \end{aligned} \quad (21)$$

To ensure that (21) is equivalent to system Equation (17), the following relationship is forced to be satisfied

$$(J_d - \mathfrak{R}_d) \frac{\partial H_d(x)}{\partial x} = -(J_a - \mathfrak{R}_a) \frac{\partial H(x)}{\partial x} + Gu, \quad (22)$$

Hence the feedback control is depicted by

$$u = \beta(x) = G^{-1} \begin{bmatrix} RP_2^* + \omega LQ_2^* + r_1(P_2^* - P_2) \\ RQ_2^* - \omega LP_2^* + r_2(Q_2^* - Q_2) \end{bmatrix}, \quad (23)$$

Furtherly it can be obtained that

$$\begin{cases} u_P = -RP_2^* - \omega LQ_2^* - r_1(P_2^* - P_2) + w_{Pu} \\ u_Q = RQ_2^* - \omega LP_2^* + r_2(Q_2^* - Q_2) - w_{Qu} \end{cases}, \quad (24)$$

With the control law in (23), it can be proved that

$$\begin{cases} \frac{\partial H_d(x)}{\partial x} = D^{-1}(x - x^*) \\ \frac{\partial^2 H_d(x)}{\partial x^2} = D^{-1} \end{cases}, \quad (25)$$

When $x = x^*$, it has $\partial H_d / \partial x = 0$ and $\partial^2 H_d / \partial x^2 > 0$, which proves that $H_d(x)$ takes the minimal value at x^* . Therefore, the minimum system energy is achieved and the closed-loop system tends to be asymptotically stable within the desired equilibrium point [23].

3.2. Robust Passivity-Based Control Strategy via Disturbance Observer

In the passivity-based control law (24), it is seen that the disturbance value w_{Pu} and w_{Qu} must be available to realize the asymptotical stability of the closed-loop system. From the definition of w_{Pu} and w_{Qu} in (10), if the unmodeled dynamics and errors (ε_P and ε_Q) are not considered, the terms w_{Pu} and w_{Qu} can be calculated through (9). Nevertheless, to improve the robustness of controller regarding to unmodeled dynamics and errors and to avoid complicated calculation of (9), terms w_{Pu} and w_{Qu} are estimated online via the double-disturbance observer (DDO) to eliminate and compensate the disturbance.

It is known that the disturbance w_{Pu} and w_{Qu} are time-varying hence they can be viewed as the polynomials with respect to time t according to Taylor's formula

$$\begin{cases} w_{Pu}(t) = p_{10} + p_{11}t + p_{12}t^2 + \dots \\ w_{Qu}(t) = p_{20} + p_{21}t + p_{22}t^2 + \dots \end{cases} \quad (26)$$

where $p_{ij}(i, j = 0, 1, 2, \dots)$ is the constant coefficient of the polynomial. As it can be seen, the dynamic behavior of the time-varying disturbance is approximated as a high-order polynomial. Nevertheless, considering that the noise becomes more serious and the structure becomes more complicated in higher order observer, a first-order observer is adopted for the disturbance observation [27]. Then the standard form of the state equation and the output equation of (11) are represented as follows

$$\begin{cases} \dot{\chi}(t) = f(\chi) + g_1(\chi)u_{PQ}(t) + g_2(\chi)w(t) \\ y(t) = \chi(t) \end{cases} \quad (27)$$

where

$$\begin{cases} \chi = \begin{bmatrix} \chi_1 & \chi_2 \end{bmatrix}^T = \begin{bmatrix} P_2 & Q_2 \end{bmatrix}^T \\ u_{PQ} = \begin{bmatrix} u_P & u_Q \end{bmatrix}^T, w = \begin{bmatrix} w_{Pu} & w_{Qu} \end{bmatrix}^T \\ f(\chi) = \begin{bmatrix} f_1(\chi) \\ f_2(\chi) \end{bmatrix} = \begin{bmatrix} -R\chi_1/L - \omega\chi_2 \\ \omega\chi_1 - R\chi_2/L \end{bmatrix} \\ g_1 = \begin{bmatrix} -1/L & 0 \\ 0 & 1/L \end{bmatrix}, g_2 = \begin{bmatrix} 1/L & 0 \\ 0 & 1/L \end{bmatrix} \end{cases} \quad (28)$$

A double-disturbance observer (DDO), which is the extension form of the observer in Reference [28], is introduced here to estimate the disturbance in (28)

$$\begin{cases} \dot{\hat{w}} = k + \mu(\chi) \\ \frac{dk}{dt} = -(\mathbf{I}(\chi)g_2(\chi))k - \mathbf{I}(\chi)[g_2(\chi)\mu(\chi) + f(\chi) + g_1(\chi)u_{PQ}] \end{cases} \quad (29)$$

where $\mu(\chi)$ and $\mathbf{I}(\chi)$ are given as

$$\begin{cases} \mu(\chi) = \begin{bmatrix} \mu_1 & \mu_2 \end{bmatrix}^T = \mathbf{I}(\chi) \cdot \chi \\ \mathbf{I}(\chi) = \begin{bmatrix} l_1 & 0 \\ 0 & l_2 \end{bmatrix} \end{cases} \quad (30)$$

If the observation error is defined as

$$\begin{cases} e_{wp} = w_{Pu} - \hat{w}_{Pu} \\ e_{wQ} = w_{Qu} - \hat{w}_{Qu} \end{cases} \quad (31)$$

Then the dynamic equation of the observation error is depicted by

$$\begin{cases} \dot{e}_{wp} + l_1 e_{wp} / L = 0 \\ \dot{e}_{wQ} + l_2 e_{wQ} / L = 0 \end{cases} \quad (32)$$

To ensure that the above disturbance equation is globally asymptotically stable, the observer gain should be chosen as $l_j > 0 (j = 1, 2)$, which means that the observation value \hat{w} can converge to the actual value exponentially. Furtherly the relationship of the estimated value and actual value of the disturbances are

$$\begin{cases} \hat{w}_{Pu}(s) = \frac{1}{1 + T_1 s} \cdot w_{Pu}(s) \\ \hat{w}_{Qu}(s) = \frac{1}{1 + T_2 s} \cdot w_{Qu}(s) \end{cases} \quad (33)$$

where $T_1 = l_1 / L$ and $T_2 = l_2 / L$; s is the differential operator. In order to realize the estimation at a certain speed and accuracy, the observer gains should be large to make the dynamic response of the observer faster than that of the control system. But the system may subject to saturation or noise during implementation if l_1 and l_2 are too large. Therefore, the observer gains need to be chosen properly to realize this balance.

In order to eliminate and compensate the disturbance, a compensation control G_{fd} is designed and added into the closed loop structure base on the estimated disturbance. The compensation control G_{fd} satisfies

$$G_{fdj}(s) = 1 + sT_j (j = 1, 2), \quad (34)$$

Along with the disturbance compensation value, the power compensation control is

$$\begin{cases} u_P = -RP_2^* - \omega LQ_2^* - r_1(P_2^* - P_2) + \hat{w}_{Pu} \cdot G_{fd1} \\ u_Q = RQ_2^* - \omega LP_2^* + r_2(Q_2^* - Q_2) - \hat{w}_{Qu} \cdot G_{fd2} \end{cases} \quad (35)$$

The overall block diagram of the proposed passivity-based control with DDO is shown in Figure 2. To apply the proposed control scheme, electrical measurements are acquired for the dq transformation and calculation of the double frequency power P_2 and Q_2 . Then the proposed passivity-based power compensation control via the disturbance observer can be realized according to the above mathematical derivation. The obtained unbalanced control signals U_{d2} and U_{q2} together with the modulation voltage signals from the common vector double loop control form the overall control scheme for VSC-HVDC under unbalanced grid conditions and finally, the voltage command for VSC converter can be available.

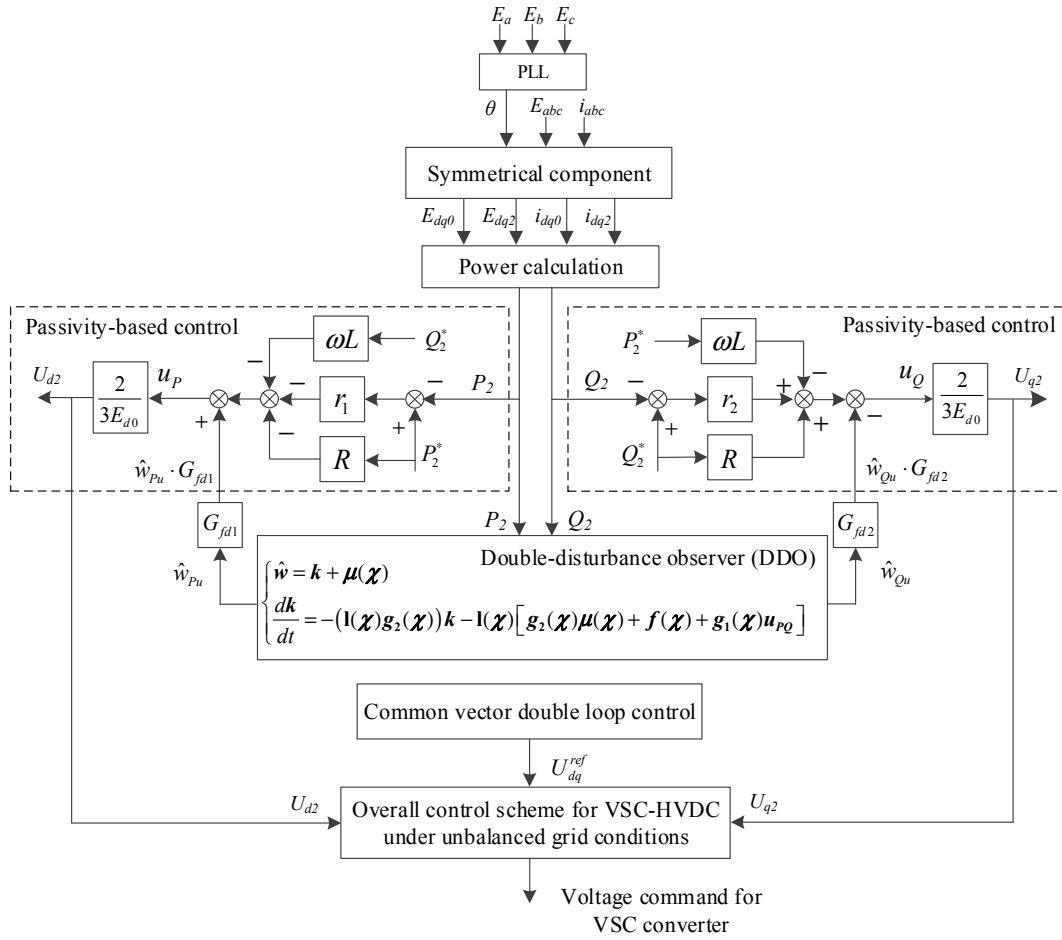


Figure 2. The block diagram of the proposed passivity-based control with DDO.

3.3. Stability Analysis of the Proposed Power Compensation Strategy via Passivity-Based Control with Disturbance Observer

The stability analysis of the proposed power compensation strategy via passivity-based control with disturbance observer is conducted in this part. From (29) and (30), the estimated disturbance value can be depicted as

$$\begin{cases} \hat{w}_{Pu}(s) = \frac{l_1(R + Ls)}{l_1 + Ls} P_2(s) + \frac{l_1 \omega L}{l_1 + Ls} Q_2(s) - \frac{l_1}{l_1 + Ls} u_P(s) \\ \hat{w}_{Qu}(s) = \frac{-l_2 \omega L}{l_2 + Ls} P_2(s) + \frac{l_2(R + Ls)}{l_2 + Ls} Q_2(s) - \frac{l_2}{l_2 + Ls} u_Q(s) \end{cases} \quad (36)$$

It can be seen in (36) that the active and reactive disturbance components are associated with both the double frequency active and reactive power, which means (36) is the MIMO (Multiple Input Multiple Output) system equation. By substituting (36) into (35), it can be obtained as

$$\begin{cases} \left(1 - \frac{l_1 G_{fd1}}{l_1 + Ls}\right) u_P(s) = -(R + r_1) P_2^*(s) - \omega L Q_2^*(s) + \left[r_1 + G_{fd1} \frac{l_1(R + Ls)}{l_1 + Ls}\right] P_2(s) + G_{fd1} \frac{l_1 \omega L}{l_1 + Ls} Q_2(s) \\ \left(1 - \frac{l_2 G_{fd2}}{l_2 + Ls}\right) u_Q(s) = -\omega L P_2^*(s) + (R + r_2) Q_2^*(s) + G_{fd2} \frac{l_2 \omega L}{l_2 + Ls} P_2(s) - \left[r_2 + G_{fd2} \frac{l_2(R + Ls)}{l_2 + Ls}\right] Q_2(s) \end{cases} \quad (37)$$

Furtherly, by substituting (37) into system Equation (11) and by replacing the state variables with the small disturbance variables, it can be depicted by

$$\begin{bmatrix} \Delta P_2 \\ \Delta Q_2 \end{bmatrix} = \mathbf{G}_M \begin{bmatrix} \Delta w_{Pu} \\ \Delta w_{Qu} \end{bmatrix}, \quad (38)$$

where Δ is defined as the small signal disturbance of each variable and G_M is derived as

$$\left\{ \begin{array}{l} \mathbf{G}_M = \begin{bmatrix} m_{11} & m_{12} \\ m_{21} & m_{22} \end{bmatrix} \\ m_{11} = \frac{(R + r_2 + Ls)(l_1 + Ls - G_{fd1} \cdot l_1)}{(l_1 + Ls)[(R + r_1 + Ls)(R + r_2 + Ls) + \omega^2 L^2]} \\ m_{12} = \frac{-\omega L(l_2 + Ls - G_{fd2} \cdot l_2)}{(l_2 + Ls)[(R + r_1 + Ls)(R + r_2 + Ls) + \omega^2 L^2]} \\ m_{21} = \frac{\omega L(l_1 + Ls - G_{fd1} \cdot l_1)}{(l_1 + Ls)[(R + r_1 + Ls)(R + r_2 + Ls) + \omega^2 L^2]} \\ m_{22} = \frac{(R + r_1 + Ls)(l_2 + Ls - G_{fd2} \cdot l_2)}{(l_2 + Ls)[(R + r_1 + Ls)(R + r_2 + Ls) + \omega^2 L^2]} \end{array} \right. , \quad (39)$$

The zero-pole theory of the MIMO system [29] points out that, for a system with transfer function matrix $G_M(s)$, the pole polynomial $\varphi(s)$ corresponding to a minimal realization is the least common denominator of all non-identically-zero minors of all orders of $G_M(s)$ and the zero polynomial $z(s)$ corresponding to a minimal realization is the greatest common divisor of all the numerators of all order- r minors of $G_M(s)$, where r is the normal rank of $G_M(s)$, provided that these minors are adjusted in such a way as to have the pole polynomial $\varphi(s)$ as their denominators. According to this theory, the zero and pole polynomials of $G_M(s)$ in (39) are

$$\left\{ \begin{array}{l} z(s) = (l_1 + Ls - G_{fd1} \cdot l_1)(l_2 + Ls - G_{fd2} \cdot l_2)[(R + r_1 + Ls)(R + r_2 + Ls) + \omega^2 L^2] \\ \varphi(s) = (l_1 + Ls)(l_2 + Ls)[(R + r_1 + Ls)(R + r_2 + Ls) + \omega^2 L^2]^2 \end{array} \right. , \quad (40)$$

Then the zero-pole map of the closed-loop system can be obtained and the system stability can be determined according to the root locus curve of the predominant pole.

When the basic parameter values in (40) are selected as stated in Section 4 for system control, the zero-pole maps of $G_M(s)$ are plotted in Figure 3. It is known from (40) that there are four poles of $G_M(s)$, among which two are determined by r_1 and r_2 (namely P_r) and two are determined by l_1 and l_2 (namely P_l). As seen in Figure 3, the poles of the closed-loop transfer function are all located in the left half of the imaginary axis and ensure a stable system. From Figure 3a,b different values of r_1 and r_2 have an effect on the pole positions of P_r and system dynamics as a result. During the increasing of r_1 and r_2 , poles P_r moves away from the imaginary axis and may be located to the two sides of real axis. Hence the dynamic response gets faster and oscillation may occur. When r_1 and r_2 get too much larger, the poles P_r are too much away from the imaginary axis and the predominant effect is attenuated. From Figure 3c,d it is seen that the observer gains l_1 and l_2 of the DDO also have impacts on system dynamic response. When l_1 and l_2 are increasing, poles P_l are located in the real axis and moves away from the imaginary axis, which means system dynamic response gets faster. The predominant poles of $G_M(s)$ are determined by the poles distribution of P_r and P_l , which indicates that proper parameters should be chosen for superior system dynamic performance.

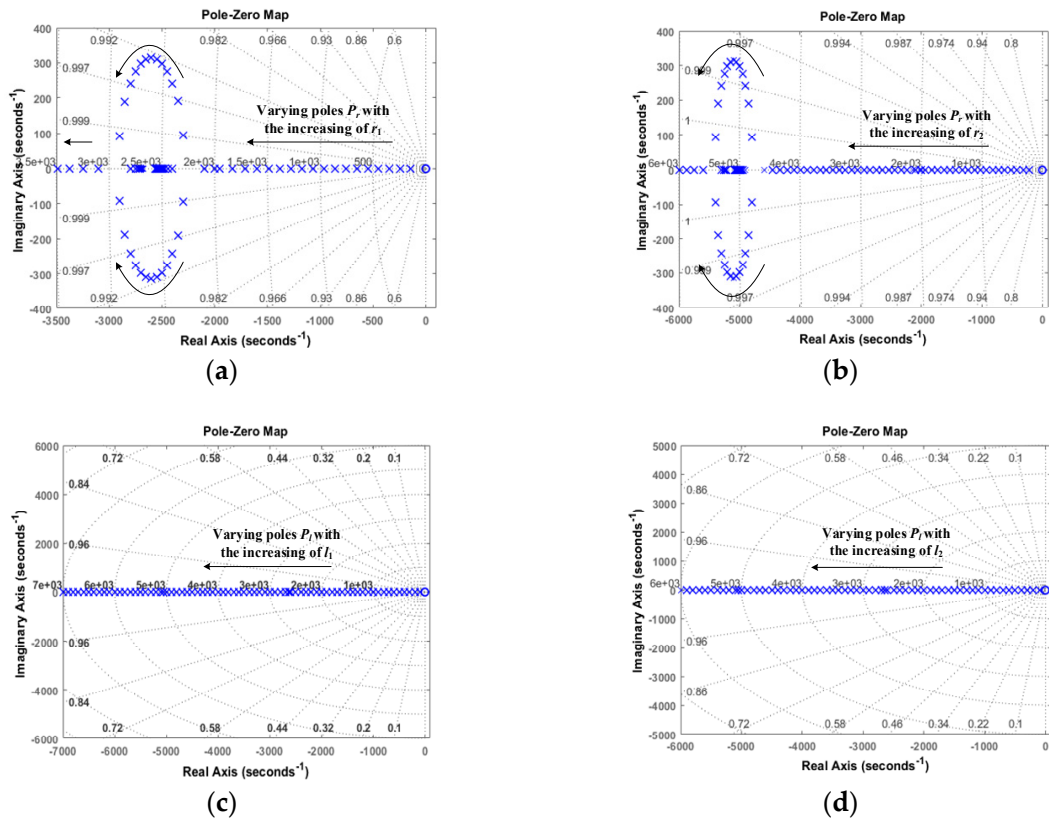


Figure 3. Zero-pole maps with different parameters. (a) Zero-pole maps with varying r_1 . (b) Zero-pole maps with varying r_2 . (c) Zero-pole maps with varying l_1 . (d) Zero-pole maps with varying l_2 .

4. Simulation Results

To verify the validity of the proposed control strategy, the dc transmission simulation model with a two-terminal VSC-based converter shown in Figure 4 is established in PSCAD/EMTDC. The rated VSC line voltage and DC bus voltage are 230 kV and 330 kV, respectively. The passivity parameters r_1 and r_2 are set as 50 and 30, while the observer gain l_1 and l_2 are set as 150 and 200. To reflect the superiority of the proposed control, the comparison cases are set in the simulations. However, since most existing control strategies are ineffectual in suppressing the active and reactive power ripples at the same time, we adopt a resonance controller with properly adjusted parameters [13] as the conventional compensation control for comparison. This resonance control is also implemented based on the double frequency ripple power control Equation (8) but superior system response cannot be achieved compared with the proposed control strategy according to the simulation results.

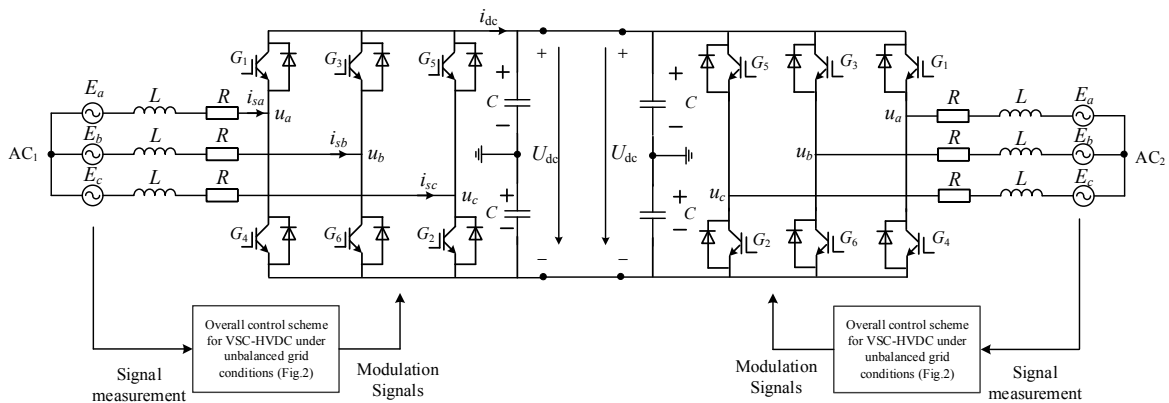


Figure 4. Simulation model with a two-terminal VSC.

4.1. Case 1

In this case, the suppression performance of the double frequency ripples with different control strategies is tested. Before 2.5 s, the system operates under normal grid condition. At time 2.5 s, the B phase and C phase voltage of source AC₂ have a drop of 4.23 kV (50%) shown in Figure 5. As for the control system, it remains unchanged with the common vector double loop control during 2.5 s to 3.5 s. After 3.5 s, the proposed power compensation strategy and the conventional resonance compensation strategy are added as the auxiliary controllers respectively for the suppression of the double frequency ripples. The simulation results are shown in Figures 6–8.

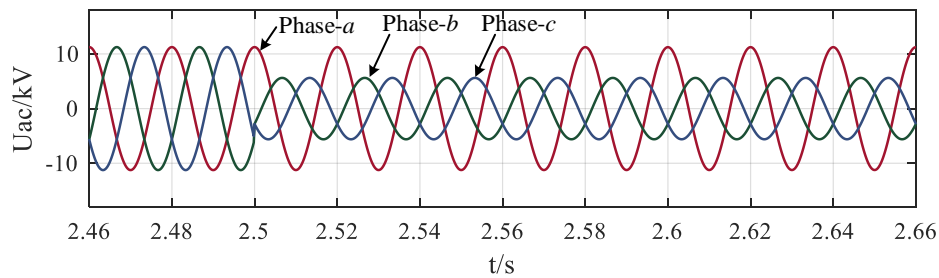


Figure 5. The three-phases voltage of source AC2.

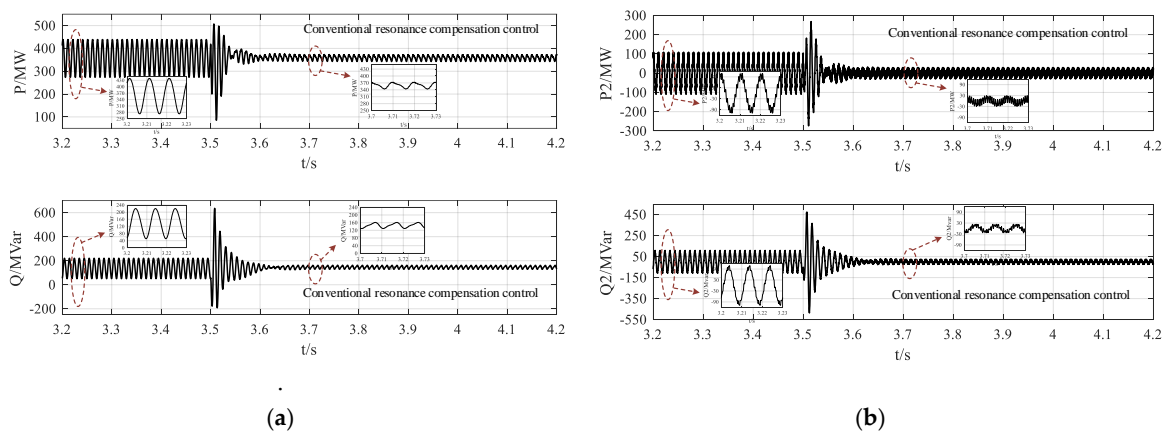


Figure 6. Simulation results with conventional resonance compensation strategy. (a) Simulation results of active and reactive power. (b) Simulation results of double frequency components of active and reactive power.

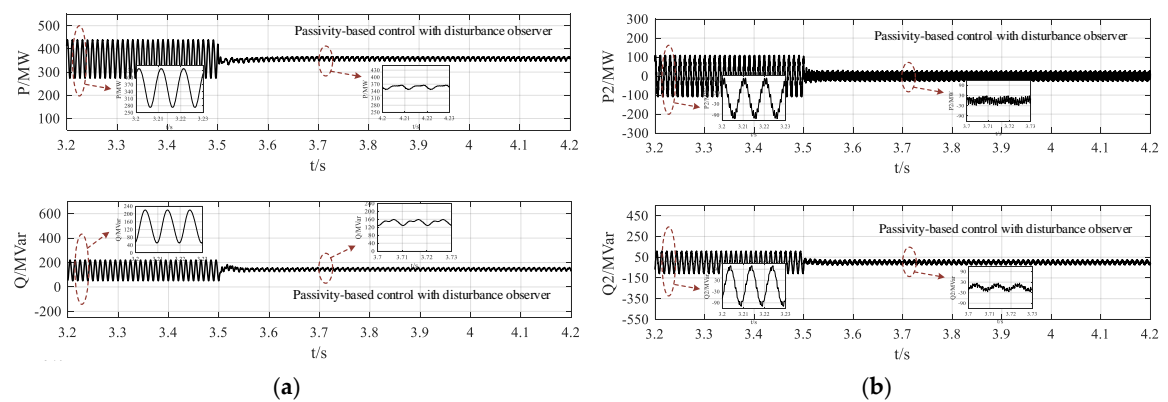


Figure 7. Simulation results with proposed passivity-based power compensation strategy via disturbance observer. (a) Simulation results of active and reactive power. (b) Simulation results of double frequency components of active and reactive power.

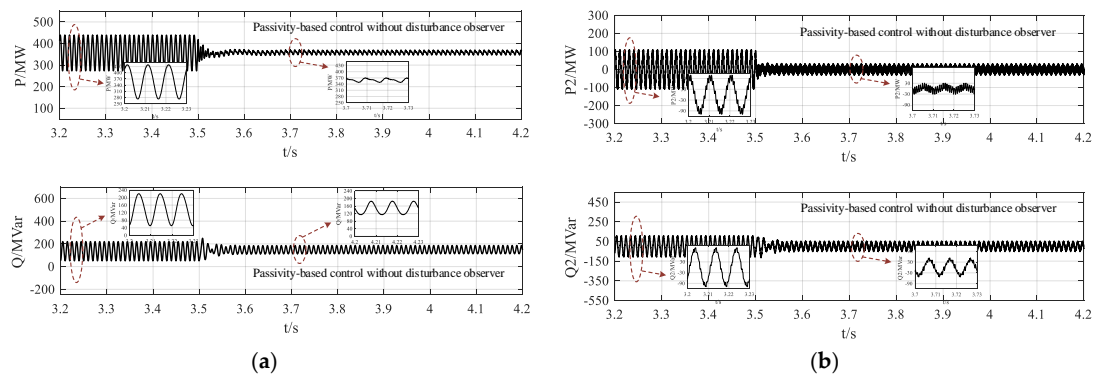


Figure 8. Simulation results with only passivity-based power compensation strategy. (a) Simulation results of active and reactive power. (b) Simulation results of double frequency components of active and reactive power.

It is seen from the simulation results that under unbalanced grid conditions with no auxiliary power compensation strategy (2.5–3.5 s), the double frequency ripples with large amplitudes appear in the active and reactive power. By comparing Figures 6 and 7, it is known that both the proposed passivity-based power compensation strategy (with the disturbance observer) and the conventional resonance compensation strategy can suppress the double frequency ripples in active and reactive power simultaneously, which verify the effectiveness of the established double frequency ripple power control Equation (8). Nevertheless, the steady-state suppression performance of the proposed strategy is better than conventional strategy through the partial enlarged figures in Figures 6 and 7. More significantly, the dynamic response at 3.5 s of the proposed compensation strategy is much better than the conventional resonance compensation strategy. Figure 6 shows that the active and reactive power reach to stable state with much large overshoot and longer transient time under the conventional strategy. Therefore, the effectiveness of the proposed passivity-based control with disturbance observer in suppressing the double frequency power ripples are verified with superior dynamic response.

To furtherly show the superior performance of the proposed passivity-based power compensation strategy with disturbance observer, the simulations with only passivity-based control is shown in Figure 8. In this scheme, the double-frequency voltage disturbances w_{Pu} and w_{Qu} are calculated through (9) instead of the observer. It can be seen from Figure 8 that the dynamic response and the suppression performance both become worse compared with that in Figure 7. The observed and calculated values of the double-frequency voltage disturbance w_{Pu} and w_{Qu} shown in Figure 9 indicate that there exists difference between the observed and calculated values caused by modelling errors and external impacts, which cause the performance degradation of the passivity-based control with calculated values of w_{Pu} and w_{Qu} . It can be concluded that the response performance of the passivity-based power compensation strategy is significantly improved with the implementation of disturbance observer.

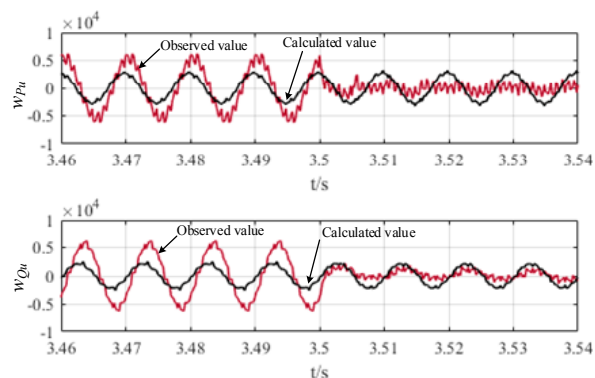


Figure 9. The observed and calculated values of the double-frequency voltage disturbance w_{Pu} and w_{Qu} .

4.2. Case 2

To verify the control effects of the proposed strategy with different control parameters, the simulation results of the double frequency power ripples (take reactive Q_2 as an example) under the proposed passivity-based power compensation strategy via disturbance observer with different parameters are shown in Figures 10 and 11.

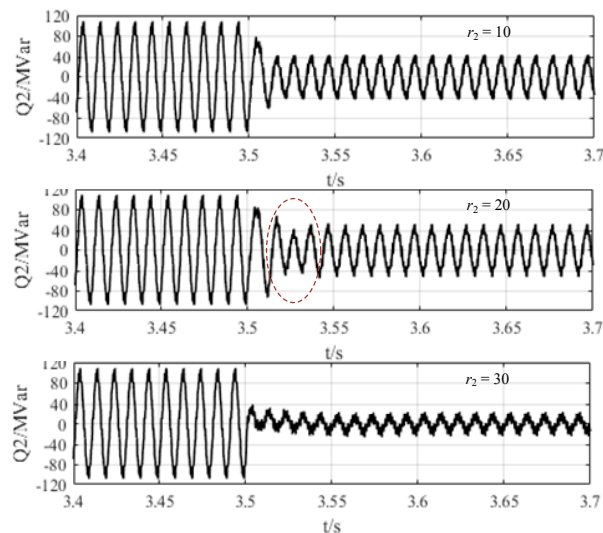


Figure 10. Simulation results of double frequency components of reactive power with different passivity parameters r_2 .

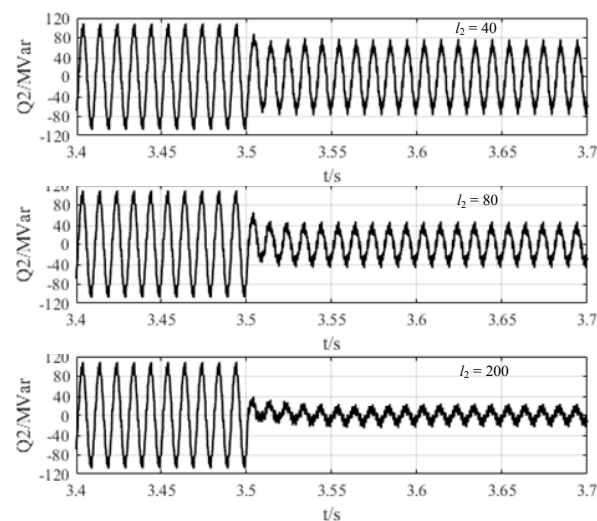


Figure 11. Simulation results of double frequency components of reactive power with different observer gain.

Figure 10 shows the simulation results of the double frequency ripples in reactive power with different passivity parameter r_2 . It indicates that during the increasing of r_2 , power oscillation may occur and the control effect is attenuated (marked in red in Figure 10) and this depends on the pole positions caused by specific value of r_2 which also confirms the previous theoretical analysis. From Figure 11, it is seen that different observer gains have significant impacts on system performance and control effects will be weakened if the observer gain is too small. Therefore, with properly chosen passivity parameters and observer gains, expected suppression performance and dynamic response can be obtained under the proposed passivity-based power compensation strategy with disturbance observer.

4.3. Case 3

In this case, the situation of single-phase grounding short-circuit fault is tested. Before 3 s, the system operates under normal condition. At time 3 s, the A phase grounding fault with the ground resistance $R_g = 0.0005 \Omega$ in AC₂. The simulation results with no auxiliary control, the conventional resonance compensation strategy and the proposed passivity-based compensation strategy via disturbance observer are shown in Figures 12–14 respectively.

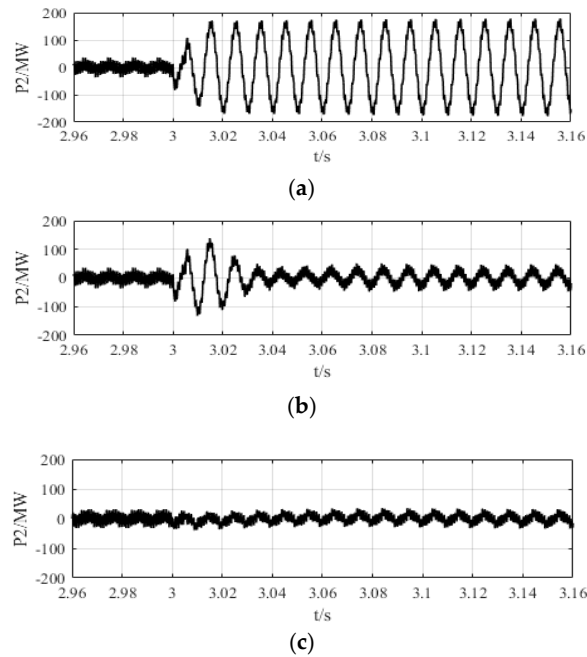


Figure 12. Simulation results of double frequency ripples in active power. (a) With no auxiliary control. (b) With conventional resonance compensation strategy. (c) With proposed passivity-based compensation strategy via disturbance observer.

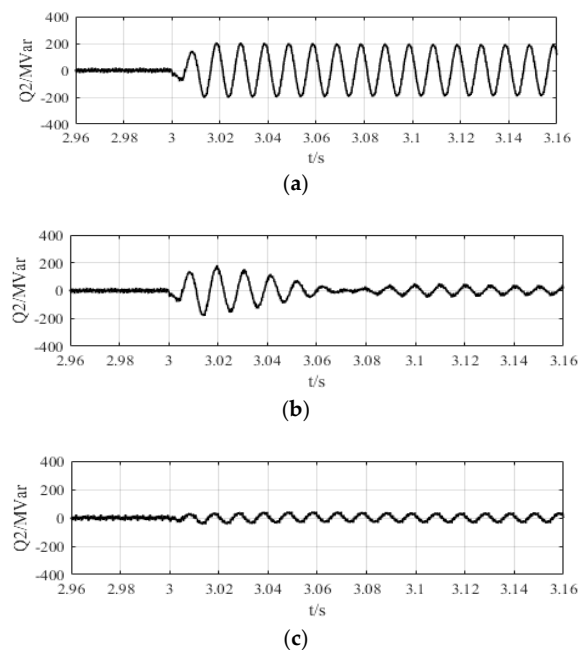


Figure 13. Simulation results of double frequency ripples in reactive power. (a) With no auxiliary control. (b) With conventional resonance compensation strategy. (c) With proposed passivity-based compensation strategy via disturbance observer.

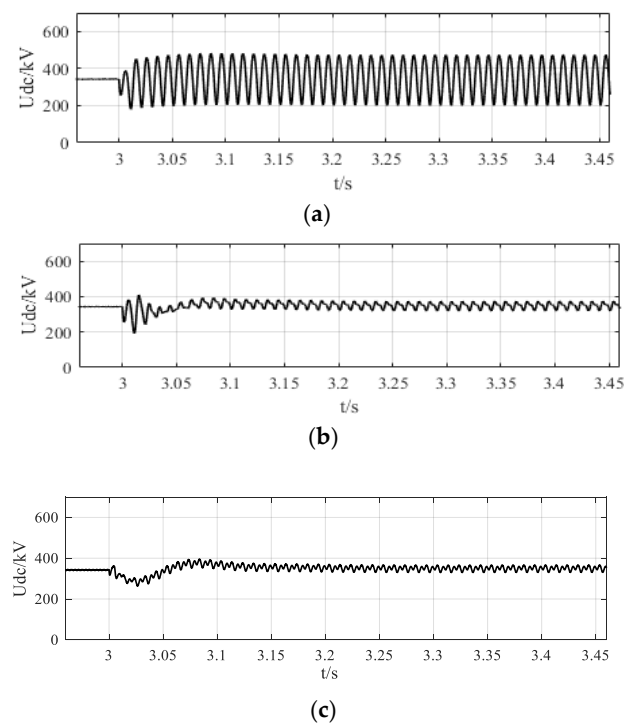


Figure 14. Simulation results of dc voltage. (a) With no auxiliary control. (b) With conventional resonance compensation strategy. (c) With proposed passivity-based compensation strategy via disturbance observer.

It is seen that under single-phase grounding short-circuit fault, large amount of double frequency ripples exists in the active and reactive with no auxiliary compensation strategy adopted, which also causes dc voltage fluctuation in double frequency. By comparing the simulation results, it can be found that double frequency ripples in active and reactive power are reduced to a large degree with the proposed compensation strategy and the suppression performance with the proposed strategy is relatively better. Additionally, the transient process at time 3 s under the proposed strategy is much improved with no overshoot and fast transient time. The response of dc voltage in Figure 14 also indicates the satisfactory dynamic performance of the system. Therefore, the proposed control shows superior properties in suppressing the double frequency power ripples and responding to external disturbance.

4.4. Comparable Evaluation

It can be concluded from the above three cases performed on the dc transmission simulation model of Figure 8 that:

(1) under the proposed control strategy, the double frequency ripples in active and reactive power are regulated with better steady-state suppression performance and enhanced dynamic response compared with the conventional resonance compensation strategy and the only passivity-based compensation strategy;

(2) different passivity parameters and different observer gains have significant impacts on system performance and control effects will be weakened if these parameters are chosen improperly;

(3) in this case of single-phase grounding short-circuit fault, the double frequency ripples in active and reactive power are reduced largely with the proposed control strategy and the transient process can be much improved with little overshoot and fast transient time.

5. Discussion

When the unbalanced grid conditions occur, the VSC converter operates in abnormal condition and the negative sequence electrical components is adverse for the system normal operation. Most exist literatures (listed in the Reference) mainly aim at obtaining some specific kind of control objective, which means the fluctuations of active and reactive power cannot be suppressed at the same time. In this case, a novel control strategy to suppress the double frequency ripples in active and reactive power of VSC-HVDC systems under unbalanced grid voltage conditions is proposed. This control strategy is based on the derived mathematical control equations of the double frequency ripple power of VSC converter. The passivity-based control together with the disturbance observer forms the basic control framework of VSC. Theoretical analysis and simulation results show that with this control, the double frequency ripples in active and reactive power of VSC-HVDC under unbalanced grid conditions are suppressed simultaneously and system performance is significantly enhanced. It should be noticed that the control parameters of the proposed strategy should be chosen properly for the desired performance response according to the respective system structure.

6. Conclusions

In this paper, the mathematical model of the double frequency ripple power for VSC-HVDC systems under unbalanced grid conditions is derived and then a power compensation strategy to suppress the double frequency ripples in active and reactive power is proposed. The main contribution of this paper is that with this proposed control strategy, the double frequency ripples in active and reactive power of VSC-HVDC under unbalanced grid conditions can be suppressed simultaneously and system performance is significantly enhanced with the implementation of the disturbance observer in the passivity-based control. The compensation strategy is proved to be effective in regulating the double frequency components of the unbalanced voltage and current without affecting the normal operation of VSC converter. The stability analysis of the proposed power compensation strategy is also conducted in this paper to analyze the system response with different control parameters. Theoretical analysis and simulations in PSCAD/EMTDC show the validity and superiority of the proposed control strategy. The research outcomes are applicative in real conditions of renewable energy generation, island network supply and microgrid, while the control parameters should be chosen carefully for the desired operation performance according to the actual system structure characteristics. The challenging issue of the application of the research outcomes is that robust PLL (Phase Locking Loop) technology should be available for accurate phase tracking under the unbalanced grid voltage conditions.

Author Contributions: Conceptualization, S.M.; Data curation, M.Z.; Investigation, T.Z., Z.F. and D.W.; Methodology, W.L.; Validation, Y.K.; Writing-original draft, Z.L.; Writing-review & editing, Z.L.

Funding: This research was funded by the Science-Tech Project of State Grid East Inner Mongolia Electric Power Research Institute [SGMDDK00D]JJS1800053]; the National Natural Science Foundation of China [51777088]; and the National Key Research and Development Program of China [2017YFB0903601].

Conflicts of Interest: The authors declare no conflict of interest.

Nomenclature

$U_{a,b,c}, i_{a,b,c}$	the three phase voltage and current of the converter
$E_{a,b,c}$	the three phase voltage of the AC grid
R, L	the per-phase resistance and inductance of the AC filter
C	the DC filter capacitor
U_{dc}, i_{dc}	the DC voltage and current of the converter
P_s, Q_s	the transmission active and reactive power of the converter
U_d, U_q	the d axis and q axis components of VSC voltage
i_d, i_q	the d axis and q axis components of VSC current
E_d, E_q	the d axis and q axis components of AC grid voltage

P_{2i}, Q_{2i}	the current-relevant components that cause the double frequency ripples in active and reactive power
P_{2u}, Q_{2u}	the voltage-relevant components that cause the double frequency ripples in active and reactive power
u_p, u_Q	the double frequency power control inputs of VSC
$J(x), J_d(x)$	the original and the desired interconnection matrix
$\mathfrak{R}(x), \mathfrak{R}_d(x)$	the original and the desired damping matrix
$H(x), H_d(x)$	the original and the desired Hamiltonian function
$G(x)$	the coefficient matrix with full rank
\hat{w}	the estimation of the disturbance
k	the internal state of the observer
$\mu(\chi), l(\chi)$	the observer function and the observer gain

References

- Shah, R.; Sánchez, J.C.; Preece, R.; Barnes, M. Stability and control of mixed AC-DC systems with VSC-HVDC: A review. *IET Gener. Transm. Dis.* **2018**, *12*, 2207–2219. [[CrossRef](#)]
- Korompili, A.; Wu, Q.; Zhao, H.Z. Review of VSC HVDC connection for offshore wind power integration. *Renew. Sustain. Energy Rev.* **2016**, *59*, 1405–1414. [[CrossRef](#)]
- Li, Y.; Tang, G.; An, T.; Pang, H.; Wang, P.; Yang, J.; Wu, Y.; He, Z. Power compensation control for interconnection of weak power systems by VSC-HVDC. *IEEE Trans. Power Del.* **2017**, *32*, 1964–1974. [[CrossRef](#)]
- Tirtashi, M.R.S.; Samuelsson, O.; Svensson, J. Impedance matching for VSC-HVDC and energy storage damping controllers. *IEEE Trans. Power Del.* **2017**, *33*, 1016–1017. [[CrossRef](#)]
- Liang, Y.; Liu, J.; Zhang, T.; Yang, Q. Arm current control strategy for MMC-HVDC under unbalanced conditions. *IEEE Trans. Power Del.* **2017**, *32*, 125–134. [[CrossRef](#)]
- Schönleber, K.; Prieto-Araujo, E.; Ratés-Palau, S.; Gomis-Bellmunt, O. Handling of unbalanced faults in HVDC-connected wind power plants. *Electr. Power Syst. Res.* **2017**, *152*, 148–159. [[CrossRef](#)]
- Schönleber, K.; Prieto-Araujo, E.; Ratés-Palau, S.; Gomis-Bellmunt, O. Extended current limitation for unbalanced faults in MMC-HVDC-connected wind power plants. *IEEE Trans. Power Del.* **2018**, *33*, 1875–1884. [[CrossRef](#)]
- Biricik, S.; Redif, S.; Ozerdem, Ö.C.; Khadem, S.K.; Basu, M. Real-time control of shunt active power filter under distorted grid voltage and unbalanced load condition using self-tuning filter. *IET Power Electron.* **2014**, *7*, 1895–1905. [[CrossRef](#)]
- Hogan, D.J.; Gonzalez-Espin, F.J.; Hayes, J.G.; Lightbody, G.; Foley, R. An adaptive digital control scheme for improved active power filtering under distorted grid conditions. *IEEE Trans. Ind. Electron.* **2017**, *65*, 988–999. [[CrossRef](#)]
- Wang, L.; Lam, C.S.; Wong, M.C. Unbalanced control strategy for a thyristor controlled LC-coupling hybrid active power filter in three -phase three-wire systems. *IEEE Trans. Power Electron.* **2016**, *32*, 1056–1069. [[CrossRef](#)]
- Guan, M.; Cheng, J.; Wang, C.; Hao, Q.; Pan, W.; Zhang, J.; Zheng, X. The frequency regulation scheme of interconnected grids with VSC-HVDC links. *IEEE Trans. Power Syst.* **2017**, *32*, 864–872. [[CrossRef](#)]
- Tirtashi, M.R.S.; Samuelsson, O.; Svensson, J.; Pates, R. Impedance matching for VSC-HVDC damping controller gain selection. *IEEE Trans. Power Syst.* **2018**, *33*, 5226–5235. [[CrossRef](#)]
- Wang, X.; Sun, D.; Zhu, Z.Q. Resonant-based backstepping direct power control strategy for DFIG under both balanced and unbalanced grid conditions. *IEEE Trans. Ind. Appl.* **2017**, *53*, 4821–4830. [[CrossRef](#)]
- Sun, L.X.; Lu, S.; Wang, Z.; Jin, Y.Q.; Chen, Q.; Yu, Y.P. Optimal control strategy of VSC-based high-voltage direct current under unbalanced grid voltage conditions. *IET Gener. Transm. Dis.* **2016**, *10*, 444–451. [[CrossRef](#)]
- Zhu, M.; Hang, L.; Li, G.; Jiang, X. Protected control method for power conversion interface under unbalanced operating conditions in AC/DC hybrid distributed grid. *IEEE Trans. Energy Convers.* **2015**, *31*, 57–68. [[CrossRef](#)]
- Jin, N.; Gan, C.; Guo, L. Predictive control of bidirectional voltage source converter with reduced current harmonics and flexible power regulation under unbalanced grid. *IEEE Trans. Energy Convers.* **2018**, *33*, 1118–1131. [[CrossRef](#)]

17. Cheng, P.; Nian, H. Direct power control of voltage source inverter in a virtual synchronous reference frame during frequency variation and network unbalance. *IET Power Electron.* **2016**, *9*, 502–511. [[CrossRef](#)]
18. Yang, W.; Zhang, A.; Li, J.; Li, G.; Zhang, H.; Wang, J. Integral plus resonant sliding mode direct power control for VSC-HVDC systems under unbalanced grid voltage conditions. *Energies* **2017**, *10*, 1528. [[CrossRef](#)]
19. Sun, L.X.; Zhu, P.F.; Wang, Z.; Chen, Y. An optimal control strategy of VSC-HVDC under unbalanced grid voltage conditions. In Proceedings of the IEEE International Conference on Cyber Technology in Automation, Control and Intelligent Systems, Shenyang, China, 8–12 June 2015.
20. Suul, J.A.; Luna, A.; Rodríguez, P. Power control of VSC HVDC converters for limiting the influence of AC unbalanced faults on multi-terminal DC grids. In Proceedings of the 10th IET International Conference on AC and DC Power Transmission (ACDC 2012), Birmingham, UK, 4–5 December 2012.
21. Wei, X.; Sun, H.; Wei, X.; Ma, Q.; Xu, F. Control strategy for VSC-HVDC power quality improvement under unbalanced grid conditions. *Int. J. Emerg. Electr. Power Syst.* **2011**, *12*, 1–22. [[CrossRef](#)]
22. Wang, X.; Blaabjerg, F.; Loh, P.C. Passivity-based stability analysis and damping injection for multi-paralleled VSCs with LCL filters. *IEEE Trans. Power Electron.* **2017**, *32*, 8922–8935. [[CrossRef](#)]
23. Meshram, R.V.; Bhagwat, M.; Khade, S.; Wagh, S.R.; Stan, A.M.; Singh, N.M. Port-controlled phasor hamiltonian modeling and IDA-PBC control of solid-state transformer. *IEEE Trans. Control Syst. Technol.* **2018**. [[CrossRef](#)]
24. Huang, J.; Wang, H.; Wang, C. Passivity-based control of a doubly fed induction generator system under unbalanced grid voltage conditions. *Energies* **2017**, *10*, 1139. [[CrossRef](#)]
25. Sang, Y.; Yang, B.; Yao, W.; Jiang, L. Design and implementation of perturbation observer-based robust passivity-based control for VSC-MTDC systems considering offshore wind power integration. *IET Gener. Transm. Dis.* **2018**, *12*, 2415–2524. [[CrossRef](#)]
26. Yang, H.; Dong, Y.; Li, W.; He, X. Average-value model of modular multilevel converters considering capacitor voltage ripple. *IEEE Trans. Power Del.* **2017**, *2*, 723–732. [[CrossRef](#)]
27. Natori, K.; Tsuji, T.; Ohnishi, K.; Hase, A.; Jezernik, K. Time-delay compensation by communication disturbance observer for bilateral teleoperation under time-varying delay. *IEEE Trans. Ind. Electron.* **2010**, *57*, 1050–1062. [[CrossRef](#)]
28. Yang, J.; Li, S.; Yu, X. Sliding-mode control for systems with mismatched uncertainties via a disturbance observer. *IEEE Trans. Ind. Electron.* **2012**, *60*, 160–169. [[CrossRef](#)]
29. Skogestad, S.; Postlethwaite, I. *Multivariable Feedback Control: Analysis and Design*; Jon Wiley & Sons: New York, NY, USA, 1988; pp. 139–141.



© 2018 by the authors. Licensee MDPI, Basel, Switzerland. This article is an open access article distributed under the terms and conditions of the Creative Commons Attribution (CC BY) license (<http://creativecommons.org/licenses/by/4.0/>).